The American Journal of Pathology, Vol. 172, No. 2, February 2008

DOI: 10.2353/ajpath.2008.070417

Musculoskeletal Pathology

Platelet Dysfunction and a High Bone Mass Phenotype in a Murine Model of Platelet-Type von Willebrand Disease

Larry J. Suva,*† Eric Hartman,* Joshua D. Dilley,† Susan Russell,* Nisreen S. Akel,*† Robert A. Skinner,† William R. Hogue,† Ulrich Budde,‡ Kottayil I. Varughese,* Taisuke Kanaji,§ and Jerry Ware*

From the Departments of Physiology and Biophysics and Orthopaedic Surgery,† Center for Orthopedic Research, Barton Research Institute, University of Arkansas for Medical Sciences, Little Rock, Arkansas; the Coagulation Laboratory,‡ Laboratory Association Professor Arndt and Partners, Hamburg, Germany; and the Department of Medicine,§ Division of Hematology, Kurume University School of Medicine, Fukuoka, Japan*

The platelet glycoprotein Ib-IX receptor binds surface-bound von Willebrand factor and supports platelet adhesion to damaged vascular surfaces. A limited number of mutations within the glycoprotein Ib-IX complex have been described that permit a structurally altered receptor to interact with soluble von Willebrand factor, and this is the molecular basis of platelet-type von Willebrand disease. We have developed and characterized a mouse model of platelet-type von Willebrand disease (G233V) and have confirmed a platelet phenotype mimicking the human disorder. The mice have a dramatic increase in splenic megakaryocytes and splenomegaly. Recent studies have demonstrated that hematopoetic cells can influence the differentiation of osteogenic cells. Thus, we examined the skeletal phenotype of mice expressing the G233V variant complex. At 6 months of age, G233V mice exhibit a high bone mass phenotype with an approximate doubling of trabecular bone volume in both the tibia and femur. Serum measures of bone resorption were significantly decreased in G233V animals. With decreased bone resorption, cortical thickness was increased, medullary area decreased, and consequently, the mechanical strength of the femur was significantly increased. Using *ex vivo* bone marrow cultures, osteoclast-specific staining in the G233V mutant marrow was diminished, whereas osteoblastogenesis was unaffected. These studies provide new insights into the relationship between the regulation of megakaryocytopoiesis and bone mass. ***(Am J Pathol 2008, 172:430–439; DOI: 10.2353/ajpath.2008.070417)***

Insights into the molecular regulation of platelet function have most often come from the characterization of human bleeding disorders that are supported with corresponding animal models.[1] Two clinically similar human bleeding disorders distinct at the molecular level, are type 2B von Willebrand disease (vWD) and platelet-type von Willebrand disease (Pt-vWD), the latter also referred to as pseudo-von Willebrand disease.[2,3] In type 2B vWD, the soluble form of von Willebrand factor (vWF) has an increased affinity for platelets and, unlike normal vWF, binds to circulating platelets via the platelet glycoprotein (GP) Ib-IX receptor complex.[4,5] The net result of this interaction is a bleeding disorder in which patients exhibit a transient or persistent thrombocytopenia and a characteristic absence of the largest vWF multimers. Similarly, a limited number of mutations within the GP Ib-IX complex have been described that permit a structurally altered receptor to interact with normal circulating vWF; this mechanism is the molecular basis of Pt-vWD.[2,6–8]

The platelet GP Ib-IX complex is synthesized from three distinct gene products, the α- and β-subunits of GP Ib and GP IX. The α-subunit of GP Ib (GP Ibα) contains all of the known ligand-binding sites within the complex with the other subunits necessary for efficient surface expression of the complex.[9,10] Mutations within the GP Ibα gene most commonly associated with Pt-vWD result in an amino acid change at position 233 (G233V or G233S) or position 239 (M239V).[6,11,12] One report describes a 27-bp deletion within the GP Ibα macroglycopeptide domain that results in a Pt-vWD phenotype.[13] Both the 233 and 239 residues reside within a β-hairpin loop in the crystal structure of GP Ibα.[14] These mutations have been

Supported by the National Heart Lung and Blood Institute (grant HL50541 to J.W.) and the Carl L. Nelson Chair of Orthopaedic Surgery.

Accepted for publication October 18, 2007.

Address reprint requests to Jerry Ware, Ph.D., Department of Physiology and Biophysics, #505, University of Arkansas for Medical Sciences, 4301 W. Markham, Little Rock, AR 72205. E-mail: jware@uams.edu.

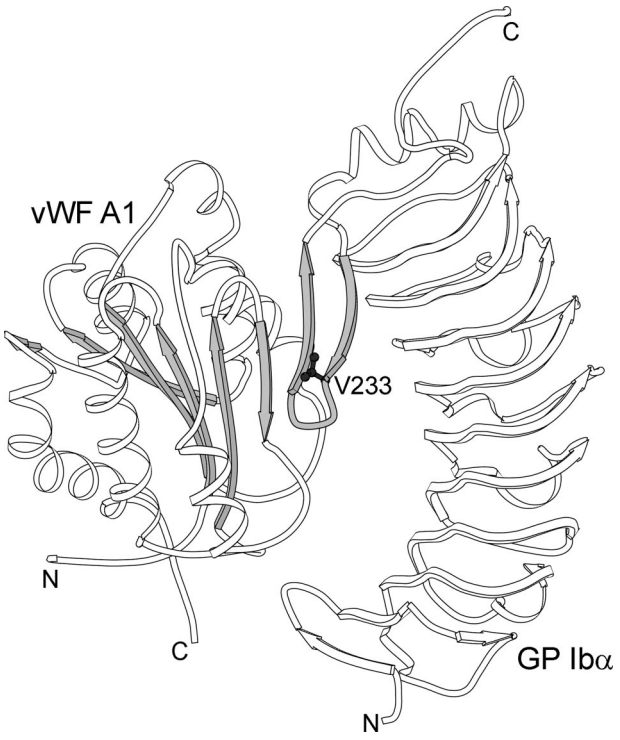

Figure 1. Pt-vWD G233V. A ribbon diagram depicting the association of GP Ibα N-terminal domain (GP IbαN) with vWF A1 domain as observed in the crystal structure.[56] GP IbαN has an elongated curved shape whereas the vWF A1 domain is rather egg shaped. GP IbαN wraps around one side of the A1 domain. The GP IbαN residues Val^{227} to Ser^{241} form a large β-loop consisting of two β-strands (shaded). These β-strands play a crucial role in binding by aligning themselves with the central β-sheet of the vWF A1 domain (also shaded). The residue mutated in Pt-vWD (G233V) is part of this loop. The presence of a Gly residue in a peptide chain adds flexibility to the peptide, and the substitution of a Val residue most likely increases the stability of the loop leading to a stronger binding. The amino and carboxyl termini of the proteins are marked as N and C.

proposed to stabilize the loop conformation leading to an increased affinity for vWF (Figure 1).[14] The exact etiology of the bleeding disorder could be the result of several factors, including the removal of the larger circulating vWF multimers from the circulation, a functional inhibition of GP Ib-IX via vWF bound to the receptor, or an inability of the mutant GP Ib-IX receptor to effectively signal after ligand binding.

Here, we describe the generation of a murine model of Pt-vWD in which a transgenic cassette expressing the human Pt-vWD point mutation (G233V) was established in a murine colony (hTg^{G233V}). A second mouse colony expressing the normal human GP Ibα subunit in platelets (hTg^{WT}) has been previously described and serves as the control for the G233V phenotype.[15] Phenotypic comparison of the two colonies confirms that the salient features of human Pt-vWD, such as impaired hemostasis, are present in the model. Histology and skeletal phenotyping of the transgenic animals revealed a significant increase in splenic megakaryocytes and the unexpected identification of a high bone mass phenotype, the result of a decrease in osteoclast number that results in an overall increase in the biomechanical strength of the femurs of hTg^{G233V} mutants. Importantly, the identification of a high bone mass phenotype as the result of an activating point mutation in the extracellular portion of the GP Ib-IX receptor extends an emerging link between megakaryocyte development and skeletal homeostasis.[16–18]

Materials and Methods

Mouse Models and Husbandry

Animals expressing a wild-type human GP Ibα transgene in the absence of mouse GP Ibα [$mGPIb\alpha^{-/-}$-$TgN(hGPIb\alpha^{WT})$ and designated hTg^{WT} have been described.[15] A variant GP Ibα transgene cassette was generated by site-directed mutagenesis replacing the Gly^{233} codon with a Val^{233} codon. Expression of the transgene used a megakaryocyte-specific promoter in a identical manner as described for hTg^{WT}[15,19,20] and was confirmed by flow cytometry using fluorescein isothiocyanate-labeled anti-human monoclonal antibodies. Multiple founders expressing the G233V transgene were initially identified, but most of the subsequent work was performed from one founder because by flow cytometry the expression of GP Ibα antigen was similar to the previously described hTg^{WT} control.[15] Expansion of the hTg^{WT} and hTg^{G233V} colonies was accomplished by breeding to a mouse GP $Ib\alpha^{Null}$ colony, a colony that has been backcrossed into the C57BL/6J strain since its inception. Briefly, hTg^{G233V} animals were generated by breeding mice expressing the mutant human transgene into a knockout colony to produce offspring with heterozygous mouse GP Ibα alleles ($mGPIb\alpha^{+/-}$) and a portion of the offspring expressing the transgene. A second generation breeding identified animals devoid of functional mouse GP Ibα alleles and still expressing the human transgene. Since the establishment of hTg^{WT} and hTg^{G233V}, both have been consistently backcrossed with C57BL/6J animals. hTg^{WT} is a congenic strain (>10 generation backcrosses). hTg^{G233V} has been backcrossed six generations. All animal handing and experimentation was performed in accordance with approved institutional guidelines and protocols.

Platelet-Rich Plasma, Platelet Counts, and Aggregation

Mouse blood was withdrawn from the retro-orbital plexus of anesthetized animals using heparin-coated microhematocrit capillaries (Fisher Scientific, Hampton, NH). Hematological parameters were determined with a Hemavet 950 (Drew Scientific, Oxford, CT) using whole blood drawn from anesthetized animals. For the generation of platelet-rich plasma blood was transferred to tubes containing heparin (Sigma, St. Louis, MO), at final concentration of 30 U/ml, or acid-citrate-dextrose at a ratio of 1:6. The blood was diluted (1:1) in modified Tyrode buffer, and platelet-rich plasma was prepared by a 10-minute centrifugation at 220 × *g*. Aggregations were performed in an aggregometer (model 500CA; Chrono-Log Corporation, Havertown, PA) and analyzed using Aggrolink software (Chrono-Log). Ristocetin was purchased from

Sigma and used at the indicated concentrations. Platelets were used at a final concentration of 3×10^5 platelets/μl in a 300-μl suspension.

Flow Cytometry

Whole blood was analyzed by flow cytometry (FACscan; Becton Dickinson, Franklin Lakes, NJ) using a phycoerythrin-labeled rat anti-mouse CD41 (anti-GPIIb or αIIb) monoclonal antibody (catalog no. 558040; BD Pharmingen, San Jose, CA) to identify the platelet population in whole blood. After identifying the platelet population, a gate was set in the flow cytometer to analyze fluorescence produced by a second labeling with a fluorescein isothiocyanate-conjugated mouse anti-human CD42b (anti-GP Ibα) monoclonal antibody (catalog no. 555472, BD Pharmingen). The absence of mouse GP Ibα expression was confirmed using a fluorescein isothiocyanate-conjugated rat anti-mouse CD42b monoclonal antibody, Xia.G5 (Emfret Analytics, Eibelstadt, Germany).

Bleeding Time Determination

Mouse tail bleeding times were determined after removal of 2 to 3 mm of distal tail. Recorded time represented the time to blood flow cessation. All bleeding time measurements were terminated at 10 minutes, and cauterization was performed to prevent death from exsanguination.

Plasma vWF Multimer Analysis

Sodium dodecyl sulfate (SDS)-agarose discontinuous gel electrophoresis was performed essentially as described with some modifications.[21] Medium (1.6%) and low resolution (1.2%) gels (LGT agarose type VII; Sigma, Munich, Germany) were prepared in running gel buffer (0.375 mol/L Tris, 0.1% SDS, pH 8.8) and cast in a 21.5 $\times$ 12.5 cm $\times$ 1.5 mm thick frame. After solidifying, a 21.5 $\times$ 2.5 cm $\times$ 1.5 mm strip of 0.8% agarose stacking gel [HGT (P) agarose; Marine Colloids, Rockland, ME] prepared in stacking gel buffer (0.125 mol/L Tris, 0,1% SDS, pH 6.8) was poured. Pooled samples of mouse plasma were diluted according to their VWF content to ~0.5 μg/ml in sample buffer (10 mmol/L Tris, 1 mmol/L ethylenediaminetetraacetic acid disodium salt, 2% SDS, pH 8.0) and incubated at 60°C for 20 minutes. Twenty-μl samples were applied to each well. The samples were electrophoresed at 60 V in Pharmacia Multiphor II electrophoresis chambers (GE Health Care, Freiburg, Germany) until the tracking dye has completely left the wells. Thereafter the wells were backfilled with the stacking gels and the electrophoresis continued at 55 V overnight until the tracking dye reached the anodal paper wick. Transfer buffer was 0.05 mol/L phosphate, pH 7.4, with 0.04 mol/L SDS, without methanol. After electrophoresis the gels were incubated for 25 minutes, before electrophoretic transfer onto nitrocellulose. Transfer was performed using a Pharmacia TE 62 tank (GE Health Care) at constant voltage of 33 V, 2 Amps (16°C, 4 hours). The filter was blocked for at least 30 minutes in low-fat (1.5%), ultra high heated milk without any additions to the dietary milk. Previous comparisons between buffered solutions prepared from low-fat dry milk and dietary low-fat milk showed no differences. After blocking the filters were incubated for 2 hours with a rabbit anti-VWF antibody (1:1000 dilution) in low-fat milk (DakoCytomation, Glostrup, Denmark). After three washings (10 minutes each) in low-fat milk, the filters were incubated with a goat anti-rabbit antibody (1:2000) in low-fat milk for 2 hours (Bio-Rad, Munich, Germany). Thereafter the filters were washed three times for 10 minutes in low-fat milk. The filters were incubated two times for a few seconds in buffer (20 mmol/L Tris/HCl, 500 mmol/L NaCl, pH 7.5) to remove the milk and thereafter placed into the dark housing of the video-detection system (Fluorchem; Alpha Innotech Corp., San Leandro, CA) consisting of a dark housing, a sensitive cooled (−30°C) charge-coupled device camera, and a special program generating 12-bit computer graphics. The filters were overlaid with a 5-ml solution containing 0.4 mg/ml luminol (Sigma-Aldrich Chemie, Steinheim, Germany), 0.01 mg/ml 4-iodophenol (Sigma-Aldrich Chemie), and 2.5 μl/ml 30% H_2O_2 (Perhydrol; Merck, Darmstadt, Germany) in Tris buffer (20 mmol/L Tris/HCl, 500 mmol/L NaCl, pH 7.5). Representative exposure times were between 30 seconds and 5 minutes.

Trabecular Bone Assessment by Micro Computed Tomography (CT)

Formalin-fixed tibiae and femora were imaged using a microCT-40 (Scanco Medical AG, Bassersdorf, Switzerland) using a voxel size of 12 μm in all dimensions. The region of interest selected for analysis comprised 240 transverse CT slices representing the entire medullary volume extending 1.24 mm distal to the end of the primary spongiosa with a border lying ~100 μm from the cortex. Three-dimensional reconstructions were created by stacking the regions of interest from each two-dimensional slice and then applying a gray-scale threshold and Gaussian noise filter as described.[22] Fractional bone volume (bone volume/tissue volume; BV/TV) and architectural properties of trabecular reconstructions (trabecular thickness (TbTh, μm), trabecular number (TbN, mm^{-1}), and connectivity density (ConnD, mm^{-3}) were calculated using published methods.[23]

Cortical Bone Assessment by MicroCT

The CT images of the mid-diaphysis of the femur and tibia were segmented into bone and marrow regions by applying a visually chosen, fixed threshold for all samples, after smoothing the image with a three-dimensional Gaussian low-pass filter. The outer contour of the bone was found automatically with the built-in Scanco iterative contouring tool. Total area was calculated by counting all voxels within the contour, bone area by counting all voxels that were segmented as bone, and marrow area was calculated as total area − bone area. This calculation was performed on all 20 slices (1 slice = 12.5 μm), using

the average for the final calculation. The outer and inner perimeter of the cortical midshaft was determined by a three-dimensional triangulation of the bone surface (BS) of the 20 slices, and cortical thickness was calculated as described.[24]

Histology

Spleens were dissected at sacrifice and fixed in 10% neutral-buffered formalin, embedded in paraffin, sectioned at 5 μm, and stained with hematoxylin and eosin (H&E). After MicroCT analysis, the same tibia and femora, fixed in 10% neutral-buffered formalin, were decalcified in 5% formic acid with agitation until deemed clear by the ammonium oxalate endpoint test.[25] The decalcified specimens were then dehydrated through graded ethanol, cleared in methyl salicylate, embedded in paraffin, sectioned (5 μm), and stained with H&E or for tartrate-resistant acid phosphatase (TRAP), as described previously.[26]

Bone Histomorphometry

Quantitation of osteoclasts was performed in sections stained for TRAP, with osteoclasts identified as $TRAP^+$ multinucleated cells, adjacent to bone. Osteoblasts were identified as layers of cuboidal cells aligned along a bone surface. All histomorphometric examination was performed in a blinded, nonbiased manner using a computerized semiautomated OsteoMeasure system (OsteoMetrics Inc., Atlanta, GA) as previously described.[22] Briefly, all measurements were confined to the secondary spongiosa and restricted to an area between 700 and 1500 μm distal to the growth plate-metaphyseal junction of the proximal tibia. A minimum of 25 fields in the proximal tibia were evaluated. Static measurements of osteoblast and osteoclast parameters were obtained as described previously[27,28] and reported using the terminology recommended by the Histomorphometry Nomenclature Committee of American Society for Bone and Mineral Research.[29]

Ex Vivo *Bone Marrow Culture*

Bone marrow cells were harvested from femurs for osteoclastogenic culture as previously described.[22,30,31] Briefly, cells were flushed from femurs, washed, and cultured in 24-well plates (Becton Dickinson Labware) at a density of 1×10^6 cells per well in α-minimal essential medium, supplemented with 15% fetal calf serum, and 10 nmol/L 1,25-dihydroxyvitamin D3 ($1,25(OH)_2D_3$) in triplicate wells per treatment. Cells were fed every 3 days with half-volumes of medium, until day 14, when cells were fixed and stained with TRAP to facilitate determination of the number of TRAP-positive multinucleated cells formed per well. For osteoblastogenesis, bone marrow cells were harvested from femurs and seeded in triplicate at 2.5×10^5 cells/cm^2 on six-well tissue culture plates (Becton Dickinson Labware) in basal medium. The total number of mesenchymal progenitors recruited into the osteoblastic lineage was measured by alkaline phosphatase-positive staining (CFU-F) at day 10. Replicate cultures were fed every 3 days with half-volumes of medium, until day 28, when cells were fixed and minerals stained with Alizarin Red to facilitate determination of the number of bone nodules (CFU-OB) formed per well.[30]

Whole Femur Mechanical Testing

Mechanical testing of intact femora was done by three-point bending as we have previously described.[32] Thawed specimens were soaked in saline for 1 hour before testing to ensure hydration and then tested at room temperature using a servohydraulic-testing machine MTS 858 Bionex test systems load frame (MTS, Eden Prairie, MN) with computer control, data logging, and calculations of load to failure using TestWorks version 4.0 (MTS). Bones were placed with their anterior side down on two horizontal supports spaced 7 mm apart; the central loading point contacted the posterior surface of the diaphysis at the midpoint of the bone length. The loading point was displaced downward (transverse to the long axis of the bone) at 0.1 mm/second until failure, generating bending in the anteroposterior plane. Load-displacement data were recorded at 100 Hz (TestWorks 4.0, MTS), and test curves were analyzed to determine measures of whole-bone strength, primarily peak load and stiffness as we have described.[32] Load to failure was recorded as the load after a 2% drop from peak load.

Statistical Analysis

All experimental data that passed standard normalization tests were analyzed by one-way analysis of variance and Student-Neuman-Keuls posthoc test. Data that were not normally distributed were analyzed by Kruskall-Wallis analysis of variance on ranks and Dunn's posthoc tests. Parametric data are presented at mean $\pm$ SEM. P values <0.05 were considered statistically significant and are reported as such.

Results

The Generation of a Murine Model of Pt-vWD

We generated a transgenic construct capable of expressing human GP Ibα in murine platelets with the normal Gly^{233} codon replaced with a Val^{233} codon. The transgenic construct contained ~2.7 kb of human DNA sequence 5′ to the human GP Ibα transcription site. We have previously reported a similar fragment expresses normal human GP Ibα on the surface of mouse platelets, and the expression pattern appears to be restricted to the megakaryocytic lineage.[19] Multiple founder transgenic animals were originally characterized for expression of the mutant human GP Ibα antigen (hTg^{G233V}).

Human Pt-vWD is an autosomal dominant disease in which platelets contain one allele product of normal GP Ibα sequence and another allele producing the mutant GP Ibα subunit. However, previous studies had confirmed that the increased affinity of the G233V substitu-

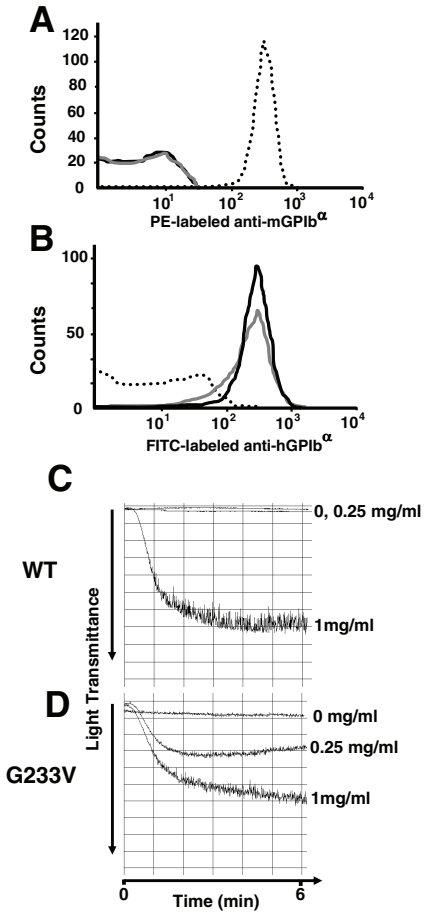

Figure 2. Flow cytometry and aggregation. Platelets from mice expressing a human GP Ibα subunit with normal sequence (WT), mice expressing a variant associated with Pt-vWF (G233V), and normal mice were analyzed by flow cytometry. **A:** An anti-mouse GP Ibα antibody reacts with the endogenous GP Ibα gene product present in normal mice (dotted line) but absent on platelets from hTg^{WT} or hTg^{G233V} animals. Both hTg^{WT} and hTg^{G233V} were derived by selective breeding to a mouse GP1bα knockout colony to eliminate the murine GP1bα gene. **B:** In contrast, hTg^{WT} (black line) and hTg^{G233V} (gray line) platelets are reactive with anti-human GP Ibα antibodies, unlike a normal mouse (dotted line). The results illustrate similar levels of surface human GP Ibα antigen expressed in the hTg^{WT} and hTg^{G233V} models. **C:** Platelets from mice expressing human GP Ibα do not agglutinate in the absence or with subthreshold levels of ristocetin (0.25 mg/ml). **D:** Mice expressing the mutation associated with Pt-vWD agglutinate with 0.25 mg/ml of ristocetin demonstrating one of the hallmark features of human Pt-vWD. All aggregation assays were supplemented with purified human plasma vWF as mentioned in the text. Tracings are representative of more than three independent agglutination assays. In the absence of supplemented human vWF no agglutination response was observed.

tion was an intrinsic property of the GP Ibα subunit and not attributable to the mixed presence of normal and mutant GP Ibα subunits.[7] Thus, to simplify the characterization of a G233V substitution, we bred transgenic animals expressing the G233V variant to animals devoid of their endogenous (murine) GP Ibα alleles.[15] This allowed a comparison of platelets expressing normal GP Ibα sequence with platelets expressing the mutant sequence. Preliminary characterization by flow cytometry revealed that the surface expression of G233V antigen was similar to the expression of the WT GP Ibα subunit in the control animals (Figure 2B). Subsequent phenotypic characterizations were performed with animals deficient in mouse GP Ibα (mGP $Ib\alpha^{-/-}$) but carrying a transgenic insertion

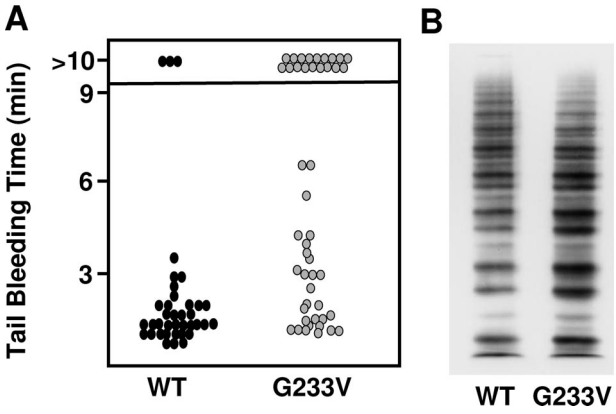

Figure 3. Tail bleeding time and multimer analysis. **A:** Tail bleeding times for individual mice are represented by the indicated data points. hTg^{G233V} mice have a pronounced defect in the hemostasis required for the cessation of blood flow (median values of 1.75 minutes versus 4.5 minutes for hTg^{WT} and hTg^{G233V}, respectively). Assays were terminated at 10 minutes and the tails of mice were cauterized. **B:** Plasma from hTg^{WT} and hTg^{G233V} mice was analyzed by SDS-agarose gel electrophoresis to visualize plasma vWF multimer structure. A slight decrease in the largest multimer species and an increase in the mid-range multimers were observed.

expressing either the normal sequence (WT) or the G233V substitution.

Hematological Consequences of a GP Ibα G233V Mutation

Circulating platelet counts were modestly reduced (20%) in animals expressing the G233V variant. The hallmark diagnostic feature of Pt-vWD is platelet agglutination with subthreshold levels of the agonist ristocetin. Shown in Figure 2 are aggregometry tracings using increasing concentrations of ristocetin. Platelet-rich plasma from hTg^{WT} animals produced agglutination using 1.0 mg/ml of ristocetin, whereas no response was observed using 0.25 mg/ml of ristocetin (Figure 2C). Platelet-rich plasma from hTg^{G233V} animals displayed agglutination with either 1 mg/ml or 0.25 mg/ml of ristocetin, albeit a diminished response (Figure 2D). Neither hTg^{WT} nor hTg^{G233V} platelets agglutinated in the absence of ristocetin. To elicit measurable agglutination, an aliquot of purified human vWF (8 μg/ml) was added to the mouse platelet-rich plasma before the addition of ristocetin. This reflects the species specificity of ristocetin-induced platelet agglutination.[33] In the absence of supplemented human von Willebrand no agglutination was observed using hTg^{WT} or hTg^{G233V} platelets (not shown).

Because human Pt-vWD presents as a bleeding phenotype,[34] we questioned whether hemostasis is impaired in mice expressing the hTg^{G233V} variant by using mouse tail bleeding time assays. The majority of animals expressing the hTg^{WT} subunit had bleeding times ranging from 1 to 3 minutes consistent with our previous characterizations of this colony (Figure 3A). Some (3 of 37) animals had extended bleeding times (Figure 3A). This has been a consistent variable most likely reflecting difficulty in reproducing the tail clip. In contrast, animals expressing the hTg^{G233V} variant subunit had a wide range of bleeding times with ~40% of the tested animals having a bleeding time of

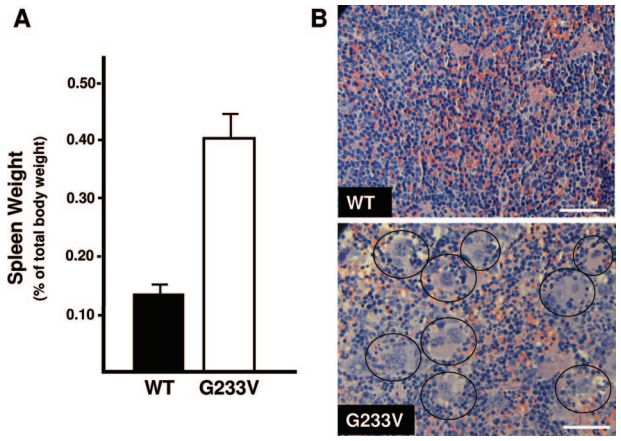

Figure 4. Splenomegaly and histology. **A:** Spleen weights from hTg^{WT} and hTg^{G233V} as a percentage of total body weight is presented. Statistically significant splenomegaly in animals harboring the G233V variant was observed ($P = 0.0004$). **B:** Representative tissue sections (H&E stained) from hTg^{WT} spleens and hTg^{G233V} spleens are shown. hTg^{G233V} spleens are dramatically enriched in megakaryocytes to the extent that the normal spleen histology of red and white pulp areas is disrupted. Representative megakaryocytes are highlighted by **circles**. Scale bars = 100 μm.

greater than 10 minutes (Figure 3A). Thus, as assayed by tail bleeding time, the hTg^{G233V} mutation is associated with increased blood loss.

Because the etiology of Pt-vWD is assumed to be related to the increased affinity between plasma vWF and circulating platelets, we assayed vWF in the plasma. As shown in Figure 3B, there is a reduction in the amount of the largest plasma vWF multimers and an apparent increase in the smaller multimers, as a consequence of the hTg^{G233V} mutation. There still appears to be sufficient vWF present in the plasma from hTg^{G233V} animals, but the loss of the more efficient large multimers may be contributing to the hemostastic abnormality.[35]

Splenomegaly in the G233V Model of Pt-vWD

On initial necropsy of animals expressing the variant GP Ib-IX, we observed splenomegaly as a consequence of the hTg^{G233V} variant. Comparing age-matched animals (12 weeks old), spleen weight as a percentage of the total mouse body weight was determined (Figure 4A). Spleens from hTg^{WT} animals were 0.14% (0.007 SEM, $n = 4$) compared to spleens from hTg^{G233V} animals, which were more than 2.5 times larger at 0.40% (0.04 SEM, $n = 7$). There was statistical significance for the increased spleen size (P value, 0.0004). Overall body weight was not significantly different between hTg^{WT} and hTg^{G233V} animals (not shown). The splenomegaly prompted us to evaluate histologically the mouse spleens, and a dramatic increase in splenic megakaryocytes was observed (Figure 4B). The increased number of megakaryocytes in spleens from hTg^{G233V} animals disrupted normal spleen histology to the extent of blurring the normal demarcation of red and white pulp regions. In contrast, bone marrow histology was unremarkable for any increase in the number of megakaryocytes or other hematopoietic cells (data not shown). Thus, the increase in splenic megakaryocytes appears to be tissue-specific.

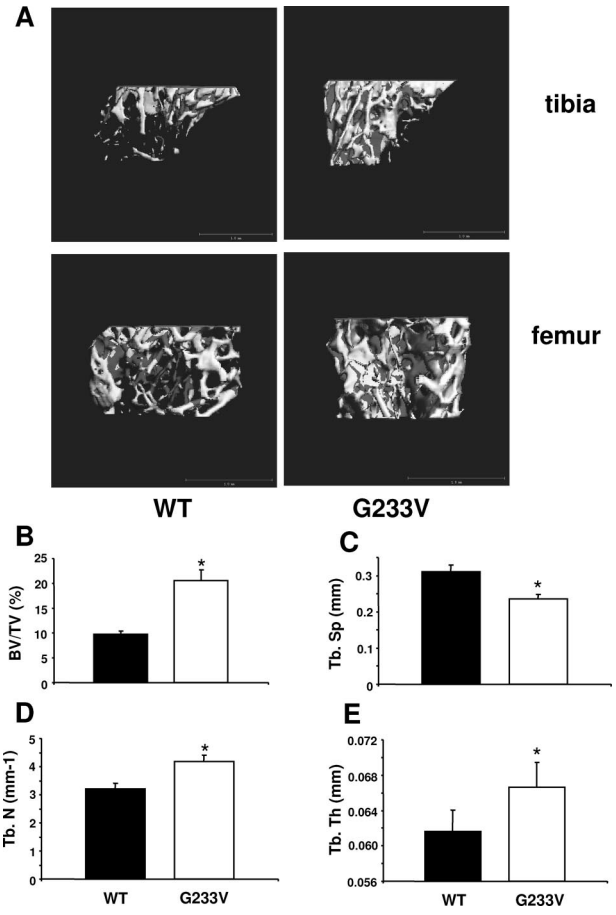

Figure 5. MicroCT analysis of bone microarchitecture. **A:** Representative microCT renderings of the trabecular region in the femur and tibia from hTg^{WT} and hTg^{G233V} mice. **B–E:** Quantitation of femur for fractional bone volume (bone volume/tissue volume, BV/TV) (**B**), trabecular separation (Tb.Sp) (**C**), trabecular number (**D**), and trabecular thickness (**E**). Measurements are from 6-month-old animals. $^*P < 0.05$.

High Bone Mass Phenotype as a Consequence of the G233V Mutation

Based on previous studies demonstrating a regulatory connection between platelet function and skeletal homeostasis,[16,18,36] we next examined the bone microarchitecture of the femur and tibia of hTg^{WT} and hTg^{G233V} mice. Gross changes in tibial and femoral morphology or bone length between the two genotypes were not apparent (data not shown). However, a significant increase in the fractional bone volume (BV/TV) of both the femur and tibia of hTg^{G233V} mice was observed (Figure 5A). In addition, and entirely consistent with the dramatic increase in BV/TV, trabecular number (Tb.N.) and trabecular thickness (Tb.Th.) are significantly increased in G233V mice, whereas trabecular separation (Tb.Sp) is significantly decreased (Figure 5, B–E). The high bone mass phenotype was evident in mice as young as 2 months (earliest age examined), progressed with age, and was evident in both genders at all time points examined (data not shown). The microCT analysis presented (Figure 5) was obtained from mice at 6 months of age.

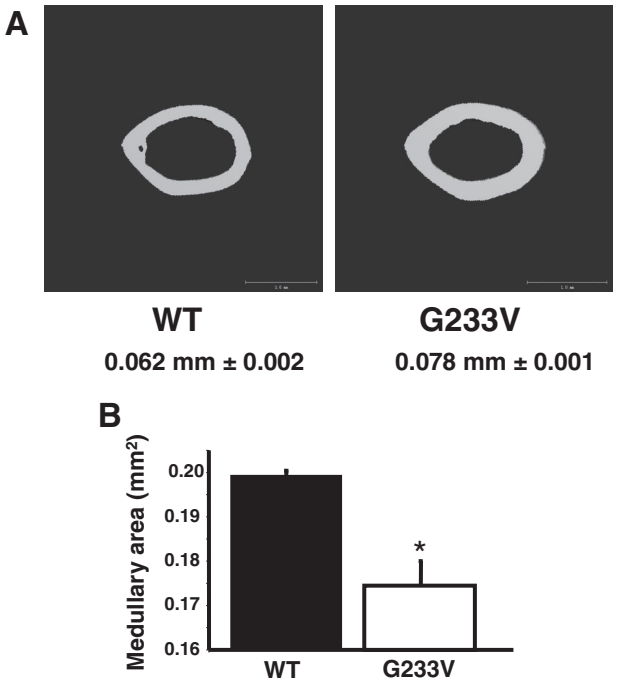

Figure 6. Cortical bone thickness. MicroCT scans of mid-diaphyseal femur was segmented into bone and marrow regions and the outer and inner contour of the bone identified as described in Materials and Methods. **A:** A representative region is shown. **B:** Cortical bone was thickened in hTg^{G233V} animals with a corresponding decreased medullary/marrow area. Data are presented as mean ± SEM ($n = 7$). *$P < 0.05$.

In addition to examining the trabecular microarchitecture, cortical bone geometry of hTg^{WT} and hTg^{G233V} mice was also examined by microCT in the mid-diaphysis of both the femur and tibia. The cortical bone cross-sectional area (CsA) of the femur or tibia was not significantly affected by the G233V mutation (data not shown). However, cortical thickness (C.Th.) of the femur was significantly increased from hTg^{WT} (0.062 ± 0.002 mm) to (0.078 ± 0.001 mm) in hTg^{G233V} mutants (Figure 6A). As a result of the significant increase in cortical thickness, medullary bone area was correspondingly significantly decreased (Figure 6B). Similar observations were made in the tibia (data not shown).

As expected, the dramatic changes in cortical geometry were also reflected in the increases in biomechanical strength of the hTg^{G233V} mutants versus hTg^{WT} femurs. Both peak load (15.61 ± 0.52 N versus 9.50 ± 0.35 N) and stiffness (61.51 ± 2.85 N/mm versus 45.27 ± 3.05 N/mm) were significantly ($P < 0.05$) increased in the hTg^{G233V} mutants compared with hTg^{WT} femurs. Taken together, these findings indicate that the femurs from hTg^{G233V} mutant mice are stronger than hTg^{WT} femurs at 6 months of age.

Consistent with the microCT evaluation, histomorphometric analysis of the long bones confirmed the increased bone volume (data not shown). Mechanistically, this was associated with a decrease in the number of osteoclasts, as measured by osteoclast surface per bone surface (OcS/BS) and the number of osteoclasts per bone perimeter (NOc/BPm), with no apparent affect on osteoblast surface per bone surface (ObS/BS) (Table 1).

Table 1. Osteoblast (Ob) and Osteoclast (Oc) Surface Numbers

	ObS/BS (%)	OcS/BS (%)	NOc/BPm
hTg^{WT}	15.7 ± 1.9	14.9 ± 1.5	8.1 ± 0.5
hTg^{G233V}	18.4 ± 1.6	11.2 ± 1.2*	6.3 ± 0.8*

Values are mean ± SEM for five mice per group.
*Significantly different from hTg^{WT}, $P < 0.05$.

No other osteoclast or osteoblast parameter measured was affected (data not shown). Consistent with both the histomorphometry and the microCT analysis, serum measures of TRAP5b, an *in vivo* biomarker of osteoclast number, revealed a significant decrease in hTg^{G233V} mice compared with WT (Figure 7A). Collectively, these data suggest that the high bone mass phenotype in hTg^{G233V} mice is the result of decreased osteoclast number.

Decreased Osteoclast Differentiation as a Consequence of the G233V Mutation

To further investigate the apparent decrease in osteoclast parameters, the number of TRAP5b-positive osteoclast-like cells formed in *ex vivo* bone marrow cultures was measured, using bone marrow derived from hTg^{WT} and hTg^{G233V} mice. Marrow was cultured in the presence of 10 nmol/L $1,25(OH)_2D_3$ and TRAP-positive cells enumerated. The number of TRAP-positive osteoclast-like cells was significantly decreased in marrow derived from hTg^{G233V} mice (Figure 7B). Osteoclasts generated from both hTg^{WT} and hTg^{G233V} mice were capable of bone resorption and no apparent differences were observed in

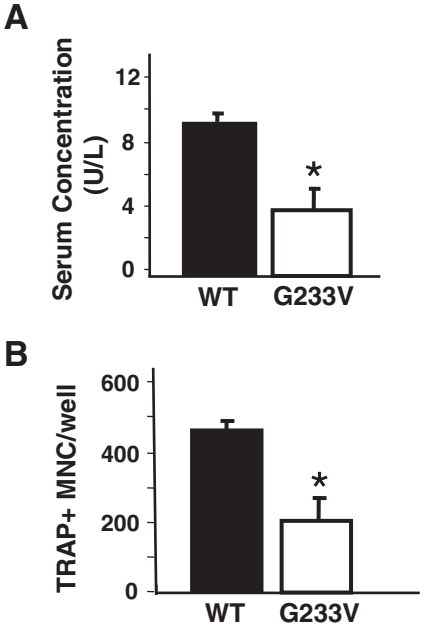

Figure 7. Serum TRAP levels and *ex vivo* osteoclast culture. **A:** Serum measures of TRAP5b, a marker of osteoclast number, are reduced in hTg^{G233V} animals. **B:** *Ex vivo* bone marrow cultures were performed (as described in Materials and Methods) and TRAP5b-positive cells were enumerated. The *ex vivo* data confirm the *in vivo* data for a decreased number of osteoclasts in hTg^{G233V} animals ($TRAP^+$ MNC, TRAP5b-positive multinucleated cells). *$P < 0.05$.

the bone resorbing capability of individual osteoclasts derived from either genotype (data not shown).

In *ex vivo* marrow cultures under osteoblastogenic conditions[30] no significant differences in colony-forming unit fibroblast (CFU-F) and colony-forming unit osteoblast (CFU-OB) were observed (data not shown). These *ex vivo* data confirm the decreased osteoclast numbers observed *in vivo* and suggest that the hTg^{G233V} mutation results in a decrease in osteoclast number, with no demonstrable effect on osteoblastic cell differentiation.

Discussion

Our original goal in this work was to generate a mouse model of Pt-vWD as a source of platelets possessing one of the gain-of-function mutations leading to increased platelet-vWF interaction. From the hemostasis perspective, the Pt-vWD mouse has several similarities with human Pt-vWD. Foremost, the animals have a bleeding phenotype, as measured by tail bleeding time assays (Figure 3), and have a severe impairment in models of thrombosis (manuscript in preparation).

Platelets from hTg^{G233V} animals display ristocetin-mediated agglutination using subthreshold levels of ristocetin, a diagnostic feature of human Pt-vWD (Figure 2). We also observed a diminished level of agglutination even with higher concentrations of ristocetin, a common feature using plasma from individuals with type 2B vWD. In plasma, Pt-vWD mice have fewer of the largest plasma vWF multimers and increased amounts of the mid-range multimers. This suggests increased vWF proteolysis, possibly by ADAMTS13.[37] Thus, a unique situation for vWF cleavage may have occurred in the hTg^{G233V} animal in which platelet-bound vWF is more susceptible to cleavage, and this is the focus of future studies. No similar situation has been reported for human Pt-vWD, but the model presented here does differ from human Pt-vWD in that a normal GP Ibα subunit is not present.

The high bone mass phenotype observed was present in both the trabecular and cortical bone compartments. Although the bone phenotype was unexpected, it was suspected once the dramatic increase in splenic megakaryocytes was observed. Indeed, three other mouse models with an increased number of megakaryocytes and an altered bone phenotype have been characterized. Two are targeted genetic deletions of transcription factors, either GATA-1 or NF-E2, both critical to the hematopoietic lineage.[16,38] The third is the overexpression of thrombopoietin leading to a myelofibrotic and osteosclerotic phenotype.[39]

Unlike the global effects that are often associated with the loss of a transcription factor, the Pt-vWD mouse is the result of a gain-of-function mutation, by a single amino acid substitution in a single gene product. It is generally believed that the GP Ib-IX receptor is exclusively expressed on the surface of platelets as a megakaryocytic-specific gene product. Our studies evaluating the expression of a GP Ib-IX complex have supported this conclusion.[19,20,40,41] Although GP Ib-IX expression by osteoclasts has not been directly examined, it seems unlikely because by transcript profiling of cells undergoing osteoclastogenesis GP IX mRNA, a required subunit for surface expression of GP Ibα, was not found.[42,43] Using immunofluorescence, we have been unable to identify expression of GP Ib-IX in osteoclasts (data not shown). Nevertheless, until proven otherwise, it is likely an oversimplification to assume that the high bone mass phenotype is the result of increased splenic megakaryocytes. Collectively, these data support the developing notion that specific links exist between platelet function and osteoclast development.

There are several mechanisms that could explain the selective increase in splenic megakaryocytes and not bone marrow megakaryocytes. One such mechanism would be rapid platelet turnover occurring in the spleen. Such turnover could be caused by mechanisms analogous to those described for type 2B vWD, in which the increased affinity between soluble ligand (vWF) and receptor leads to microaggregates and clearance from the blood.[44] Surprisingly, such a result might be expected to increase splenic phagocytes but not megakaryocytes. In addition, the observed increased in splenic megakaryocytes might be explained by two different scenarios. One locally high concentrations of Tpo in the spleen and a local environment highly conducive to megakaryocyte maturation and differentiation may have been generated. Alternatively, a change in marrow architecture that accompanies the observed change in trabecular bone architecture and geometry may have impaired normal marrow megakaryocytopoiesis. As a consequence, extramedullary hematopoiesis in the spleen has increased. Indeed, it has been recently reported that type 2B vWF impairs human bone marrow megakaryocytopoiesis as determined by ultrastructural changes in bone marrow megakaryocytes.[45] If a similar situation occurs in Pt-vWD, perhaps the mouse spleen is compensating for a defect in the bone marrow.

Collectively, these data raise an intriguing question, is the high bone mass phenotype reported here a direct result of this gain-of-function mutation or a secondary phenotype caused by the increase in splenic megakaryocytes? Both GATA-1 and NF-E2 knockout mice have a significant reduction in platelet GP Ib-IX expression with a characterized GATA-1 *cis*-acting element in the GP Ibα promoter.[46–48] We have been unable to demonstrate any skeletal phenotype in mice completely lacking the (GP) Ib-IX receptor (J.W. and L.J.S., unpublished observations). This implies that the observed pathology is most likely not a direct result of vWF binding to platelets. It is currently not known if the Pt-vWD mutation directly influences the osteoclast or if the simple overproduction of splenic megakaryocytes in this model leads to the profound trabecular and cortical bone changes observed in these mice.

Recent evidence has linked megakaryocytes to the regulation of osteoclast differentiation and function.[18] Pt-vWD mice have decreased osteoclastogenic potential compared to control mice, but the osteoclasts formed are capable of bone resorption. Together, with the *in vivo* observations of increased megakaryocyte number, these results imply that megakaryocytes may produce a systemic factor(s) that regulates osteoclast development

and thereby bone mass. The mechanism responsible for the suppression of osteoclastogenesis is unknown. Some have suggested that platelets and megakaryocytes express osteoprotegerin and RANKL,[49] but the reliability of commercially available osteoprotegerin assays seem problematic.[50] Kacena and colleagues[18] reported that both megakaryocytes and their conditioned medium could inhibit osteoclast development by up to 10-fold, but the identity of the inhibitory factor(s) remains unknown, despite attempts to evaluate endogenous inhibitors such as osteoprotegerin.[36] Other studies have demonstrated the expression of bone morphogenetic proteins (BMPs) by megakaryocytes.[51,52] GATA-1^{low} mice have increased levels of BMPs coinciding with an increased number of bone marrow megakaryocytes.[52] BMP production by megakaryocytes does represent such a candidate because osteoclasts are known to possess BMP receptors and are stimulated by BMPs.[53–55] Whether BMP expression explains the bone phenotype in the hTg^{G233V} model can be examined in future studies.

The generation and characterization of the Pt-vWD mouse provides two interesting but quite different avenues for future research. First, what are the important hemostasis issues regarding how Pt-vWD leads to such a severe bleeding phenotype? Does vWF bound to the receptor on circulating platelets represent an *in vivo* blockade of GP Ib-IX? Are Pt-vWD platelets capable of normal platelet activation? Does the structurally abnormal GP Ib-IX receptor associated with Pt-vWD present neoepitopes analogous to ligand-induced binding sites described for integrin receptors? Finally, we consider the Pt-vWD phenotype as an important model in which to define further the link between megakaryocytes, osteoclastogenesis, and bone physiology. Such studies are currently the focus of intensive ongoing investigation in our laboratory.

References

1. Ware J: Dysfunctional platelet membrane receptors: from humans to mice. Thromb Haemost 2004, 92:478–485
2. Miller JL, Castella A: Platelet-type von Willebrand's disease: characterization of a new bleeding disorder. Blood 1982, 60:790–794
3. Miller JL, Kupinski JM, Castella A, Ruggeri ZM: von Willebrand factor binds to platelets and induces aggregation in platelet-type but not type IIB von Willebrand disease. J Clin Invest 1983, 72:1532–1542
4. Nichols WC, Cooney KA, Ginsburg D, Ruggeri ZM: von Willebrand disease. Thrombosis and Hemorrhage. Edited by Loscalzo J, Schafer AI. Baltimore, Williams & Wilkins 1998, pp 729–756
5. Sadler JE: Biochemistry and genetics of von Willebrand factor. Annu Rev Biochem 1998, 67:395–424
6. Miller JL, Cunningham D, Lyle VA, Finch CL: Mutation in the gene encoding the α chain of platelet glycoprotein Ib in platelet-type von Willebrand disease. Proc Natl Acad Sci USA 1991, 88:4761–4765
7. Murata M, Russell SR, Ruggeri ZM, Ware J: Expression of the phenotypic abnormality of platelet-type von Willebrand disease in a recombinant glycoprotein Ibα fragment. J Clin Invest 1993, 91:2133–2137
8. Moriki T, Murata M, Kitaguchi T, Anbo H, Handa M, Watanabe K, Takahashi H, Ikeda Y: Expression and functional characterization of an abnormal platelet membrane glycoprotein Ib alpha (Met239->Val) reported in patients with platelet-type von Willebrand disease. Blood 1997, 90:698–705
9. López JA, Leung B, Reynolds CC, Li CQ, Fox JEB: Efficient plasma membrane expression of a functional platelet glycoprotein Ib-IX complex requires the presence of its three subunits. J Biol Chem 1992, 267:12851–12859
10. Andrews RK, Gardiner EE, Shen Y, Whisstock JC, Berndt MC: Glycoprotein Ib-IX-V. Int J Biochem Cell Biol 2003, 35:1170–1174
11. Takahashi H, Murata M, Furukawa T, Handa M, Watanabe K, Ikeda Y: A point mutation in gene encoding glycoprotein IBα in a Japanese family with platelet-type von Willebrand disease. Blood 1992, 80:130a
12. Matsubara Y, Murata M, Sugita K, Ikeda Y: Identification of a novel point mutation in platelet glycoprotein Ibα. Gly to Ser at residue 233, in a Japanese family with platelet-type von Willebrand disease. J Thromb Haemost 2003, 1:2198–2205
13. Othman M, Notley C, Lavender FL, White H, Byrne CD, Lillicrap D, O'Shaughnessy DF: Identification and functional characterization of a novel 27-bp deletion in the macroglycopeptide-coding region of the GPIBA gene resulting in platelet-type von Willebrand disease. Blood 2005, 105:4330–4336
14. Huizinga EG, Tsuji S, Romijn RA, Schiphorst ME, de Groot PG, Sixma JJ, Gros P: Structures of glycoprotein Ibalpha and its complex with von Willebrand factor A1 domain. Science 2002, 297:1176–1179
15. Ware J, Russell S, Ruggeri ZM: Generation and rescue of a murine model of platelet dysfunction: the Bernard-Soulier syndrome. Proc Natl Acad Sci USA 2000, 97:2803–2808
16. Kacena MA, Gundberg CM, Nelson T, Horowitz MC: Loss of the transcription factor p45 NF-E2 results in a developmental arrest of megakaryocyte differentiation and the onset of a high bone mass phenotype. Bone 2005, 36:215–223
17. Beeton CA, Bord S, Ireland D, Compston JE: Osteoclast formation and bone resorption are inhibited by megakaryocytes. Bone 2006, 39:985–990
18. Kacena MA, Nelson T, Clough ME, Lee SK, Lorenzo JA, Gundberg CM, Horowitz MC: Megakaryocyte-mediated inhibition of osteoclast development. Bone 2006, 39:991–999
19. Ware J, Russell SR, Marchese P, Ruggeri ZM: Expression of human platelet glycoprotein Ibα in transgenic mice. J Biol Chem 1993, 268:8376–8382
20. Fujita H, Hashimoto Y, Russell S, Zieger B, Ware J: In vivo expression of murine platelet glycoprotein Ibα. Blood 1998, 92:488–495
21. Budde U, Schneppenheim R, Plendle H, Dent J, Ruggeri ZM, Zimmerman TS: Luminographic detection of von Willebrand factor multimers in agarose gels and on nitrocellulose membranes. Thromb Haemost 1990, 63:312–315
22. Rzonca SO, Suva LJ, Gaddy D, Montague DC, Lecka-Czernik B: Bone is a target for the antidiabetic compound rosiglitazone. Endocrinology 2004, 145:401–406
23. Hildebrand T, Laib A, Muller R, Dequeker J, Ruegsegger P: Direct three-dimensional morphometric analysis of human cancellous bone: microstructural data from spine, femur, iliac crest, and calcaneus. J Bone Miner Res 1999, 14:1167–1174
24. Bagi CM, Hanson N, Andresen C, Pero R, Lariviere R, Turner CH, Laib A: The use of micro-CT to evaluate cortical bone geometry and strength in nude rats: correlation with mechanical testing, pQCT and DXA. Bone 2006, 38:136–144
25. Skinner R, Hickmon S, Lumpkin CJ, Aronson J, Nicholas R: Twenty years of successful specimen management. J Histotechnol 1997, 20:267–277
26. Bendre MS, Gaddy-Kurten D, Mon-Foote T, Akel NS, Skinner RA, Nicholas RW, Suva LJ: Expression of interleukin 8 and not parathyroid hormone-related protein by human breast cancer cells correlates with bone metastasis in vivo. Cancer Res 2002, 62:5571–5579
27. Suva LJ, Seedor JG, Endo N, Quartuccio HA, Thompson DD, Bab I, Rodan GA: Pattern of gene expression following rat tibial marrow ablation. J Bone Miner Res 1993, 8:379–388
28. Perrien DS, Akel NS, Dupont-Versteegden EE, Skinner RA, Siegel ER, Suva LJ, Gaddy D: Aging alters the skeletal response to disuse in the rat. Am J Physiol 2007, 292:R988–R996
29. Parfitt AM, Drezner MK, Glorieux FH, Kanis JA, Malluche H, Meunier PJ, Ott SM, Recker RR: Bone histomorphometry: standardization of nomenclature, symbols, and units. Report of the ASBMR Histomorphometry Nomenclature Committee. J Bone Miner Res 1987, 2:595–610
30. Gaddy-Kurten D, Coker JK, Abe E, Jilka RL, Manolagas SC: Inhibin suppresses and activin stimulates osteoblastogenesis and osteoclastogenesis in murine bone marrow cultures. Endocrinology 2002, 143:74–83

31. Lazarenko OP, Rzonca SO, Hogue WR, Swain FL, Suva LJ, Lecka-Czernik B: Rosiglitazone induces decreases in bone mass and strength that are reminiscent of aged bone. Endocrinology 2007, 148:2669–2680
32. Perrien DS, Akel NS, Edwards PK, Carver AA, Bendre MS, Swain FL, Skinner RA, Hogue WR, Nicks KM, Pierson TM, Suva LJ, Gaddy D: Inhibin A is an endocrine stimulator of bone mass and strength. Endocrinology 2007, 148:1654–1665
33. Scott JP, Montgomery RR, Retzinger GS: Dimeric ristocetin flocculates proteins, binds to platelets, and mediates von Willebrand factor-dependent agglutination of platelets. J Biol Chem 1991, 266:8149–8155
34. Miller JL: Platelet-type von Willebrand disease. Thromb Haemost 1996, 75:865–869
35. Sporn LA, Marder VJ, Wagner DD: Inducible secretion of large, biologically potent von Willebrand factor multimers. Cell 1986, 46:185–190
36. Kacena MA, Gundberg CM, Horowitz MC: A reciprocal regulatory interaction between megakaryocytes, bone cells, and hematopoietic stem cells. Bone 2006, 39:978–984
37. Bowen DJ, Collins PW: Insights into von Willebrand factor proteolysis: clinical implications. Br J Haematol 2006, 133:457–467
38. Kacena MA, Shivdasani RA, Wilson K, Xi Y, Troiano N, Nazarian A, Gundberg CM, Bouxsein ML, Lorenzo JA, Horowitz MC: Megakaryocyte-osteoblast interaction revealed in mice deficient in transcription factors GATA-1 and NF-E2. J Bone Miner Res 2004, 19:652–660
39. Yan XQ, Lacey D, Hill D, Chen Y, Fletcher F, Hawley RG, McNiece IK: A model of myelofibrosis and osteosclerosis in mice induced by overexpressing thrombopoietin (mpl ligand): reversal of disease by bone marrow transplantation. Blood 1996, 88:402–409
40. Zieger B, Hashimoto Y, Ware J: Alternative expression of platelet glycoprotein Ibβ mRNA from an adjacent 5′ gene with an imperfect polyadenylation signal sequence. J Clin Invest 1997, 99:520–525
41. Ware J: Molecular analyses of the platelet glycoprotein Ib-IX-V receptor. Thromb Haemost 1998, 79:466–478
42. Cappellen D, Luong-Nguyen NH, Bongiovanni S, Grenet O, Wanke C, Susa M: Transcriptional program of mouse osteoclast differentiation governed by the macrophage colony-stimulating factor and the ligand for the receptor activator of NFkappa B. J Biol Chem 2002, 277:21971–21982
43. Ishida N, Hayashi K, Hoshijima M, Ogawa T, Koga S, Miyatake Y, Kumegawa M, Kimura T, Takeya T: Large scale gene expression analysis of osteoclastogenesis in vitro and elucidation of NFAT2 as a key regulator. J Biol Chem 2002, 277:41147–41156
44. Ware J, Dent JA, Azuma H, Sugimoto M, Kyrle PA, Yoshioka A, Ruggeri ZM: Identification of a point mutation in type IIB von Willebrand disease illustrating the regulation of von Willebrand factor affinity for the platelet GP Ib-IX receptor. Proc Natl Acad Sci USA 1991, 88:2946–2950
45. Nurden P, Debili N, Vainchenker W, Bobe R, Bredoux R, Corvazier E, Combrie R, Fressinaud E, Meyer D, Nurden AT, Enouf J: Impaired megakaryocytopoiesis in type 2B von Willebrand disease with severe thrombocytopenia. Blood 2006, 108:2587–2595
46. Hashimoto Y, Ware J: Identification of essential GATA and Ets binding motifs within the promoter of the platelet glycoprotein Ibα gene. J Biol Chem 1995, 270:24532–24539
47. Vyas P, Ault K, Jackson CW, Orkin SH, Shivdasani RA: Consequences of GATA-1 deficiency in megakaryocytes and platelets. Blood 1999, 93:2867–2875
48. Shivdasani RA: The role of transcription factor NF-E2 in megakaryocyte maturation and platelet production. Stem Cells 1996, 14:112–115
49. Bord S, Frith E, Ireland DC, Scott MA, Craig JI, Compston JE: Megakaryocytes modulate osteoblast synthesis of type-I collagen, osteoprotegerin, and RANKL. Bone 2005, 36:812–819
50. Rogers A, Eastell R: Circulating osteoprotegerin and receptor activator for nuclear factor kappaB ligand: clinical utility in metabolic bone disease assessment. J Clin Endocrinol Metab 2005, 90:6323–6331
51. Sipe JB, Zhang J, Waits C, Skikne B, Garimella R, Anderson HC: Localization of bone morphogenetic proteins (BMPs)-2, -4, and -6 within megakaryocytes and platelets. Bone 2004, 35:1316–1322
52. Garimella R, Kacena MA, Tague SE, Wang J, Horowitz MC, Anderson HC: Expression of bone morphogenetic proteins and their receptors in the bone marrow megakaryocytes of GATA-1(low) mice: a possible role in osteosclerosis. J Histochem Cytochem 2007, 55:745–752
53. Kaneko H, Arakawa T, Mano H, Kaneda T, Ogasawara A, Nakagawa M, Toyama Y, Yabe Y, Kumegawa M, Hakeda Y: Direct stimulation of osteoclastic bone resorption by bone morphogenetic protein (BMP)-2 and expression of BMP receptors in mature osteoclasts. Bone 2000, 27:479–486
54. Wutzl A, Brozek W, Lernbass I, Rauner M, Hofbauer G, Schopper C, Watzinger F, Peterlik M, Pietschmann P: Bone morphogenetic proteins 5 and 6 stimulate osteoclast generation. J Biomed Mater Res A 2006, 77:75–83
55. Okamoto M, Murai J, Yoshikawa H, Tsumaki N: Bone morphogenetic proteins in bone stimulate osteoclasts and osteoblasts during bone development. J Bone Miner Res 2006, 21:1022–1033
56. Huizinga EG, Tsuji S, Romijn RA, Schiphorst ME, de Groot PG, Sixma JJ, Gros P: Structures of glycoprotein Ibalpha and its complex with von Willebrand factor A1 domain. Science 2002, 297:1176–1179